SPECTRAL RESPONSE OF MICROBOLOMETERS FOR HYPERSPECTRAL IMAGING

A FINAL REPORT SUBMITTED TO THE GRADUATE DIVISION OF THE UNIVERSITY OF HAWAI'I AT MĀNOA IN PARTIAL FULFILLMENT OF THE REQUIREMENTS FOR THE DEGREE OF

MASTER OF SCIENCE

IN

GEOLOGY AND GEOPHYSICS

NOVEMBER 2017

BY

CASEY I. HONNIBALL

COMMITTEE:

ROBERT WRIGHT
PAUL G. LUCEY
PAUL WESSEL

Keywords: Microbolometer, Hyperspectral imaging, Long-wave infrared, Mid-wave infrared, Vanadium Oxide, Amorphous Silicon, Spectral response

ABSTRACT

Hyperspectral imaging (HSI) is a technique with a growing list of applications and potential users. This technique combines the power of imaging with the chemical discrimination of spectroscopy. Because HSI divides light from the scene into narrow slices of wavelength, the technique typically employs cryogenic detector arrays to achieve needed sensitivity. However, within the last two decades, microbolometer arrays have improved in sensitivity, pixel count and total array area. At the University of Hawai'i at Manoa, we have shown that when paired with interferometer spectrometers to maximize performance, microbolometer arrays can provide sufficient sensitivities for a variety of infrared HSI applications. The ability of microbolometer arrays to operate at ambient-temperature make them attractive candidates for low power applications, including space-based instruments on small satellites. Under two NASA projects we are determining the suitability of uncooled microbolometers for HSI systems with the aim of HSI measurements from smaller satellites than is possible with cryogenic instruments. The suitability of a detector is governed in part by its spectral response. Microbolometers have wide variations in spectral response by technology and vendor; as part of our NASA projects we conducted a spectral response measurement campaign on four different microbolometer cameras and one cooled photon detector. Three of the microbolometers are sensitive to the long-wave infrared from 7.5 to 14 microns (two cameras from FLIR and one from Sofradir EC) and the fourth is sensitive to both the mid-wave and long-wave infrared regions from 3 to 14 microns (from INO). The cooled photon detector camera is indium antimonide (from IRCamera) sensitive to the mid-wave infrared from 2 to 5.2 microns. The spectral response of all the cameras tested is presented. We find that the INO microbolometer provides the highest sensitivity of all the cameras and shows a flat spectral response across the whole wavelength range.

Table of Contents

List of Figures

List of Tables

INTRODUCTION

There are many kinds of infrared imaging detectors including; thermocouples and thermopiles, bolometers, and imagers developed to use the photoelectric effect (Einstein, 1905) in the form of large arrays of photodiodes. These photodiode arrays were the most common type of infrared array detectors until about 2000. However, at infrared wavelengths thermal agitation of the lattice produces a flow of dark current that is indistinguishable from current from photons, so photoelectric (photon) detectors must be cooled to very low, cryogenic temperatures to operate. A recently developed alternative to photon detectors are bolometers. Bolometers measure infrared radiation by detecting the change in electrical properties caused by an infrared photon heating the detector material. Large arrays of tiny bolometers (microbolometers) are now a common infrared imaging technology and are typically used for thermal imaging of a variety of Earth and space applications. In the past few decades uncooled microbolometers have realized significant technological advances including improved reliability in manufacturing, higher resolution, decreased pixel pitch, and increased array area. These advances have led to lower costs and therefore wide availability and accessibility. Commonly used infrared detecting materials for microbolometers are Amorphous Silicon (a-Si) and Vanadium Oxide (VOx), with VOx leading sensitivity, while a-Si is less costly (Petitweg, 2008). Consumers may now choose from a variety of configurations for microbolometer arrays, from small arrays of 64x128 pixels to high definition sizes of 1024x768, from 17 μm to 50 μm pixels, and to which detector technology is used.

The improved sensitivity of microbolometers has enabled a wider range of science application than simple imaging. In Hawai'i, we have been investigating and developing the use of uncooled microbolometers for hyperspectral imaging (HSI). Hyperspectral images contain spectral information for each object in the image. Infrared instruments utilizing microbolometers are light weight, low cost, and feature a smaller footprint than instruments that employ detector technologies that require cryogenic cooling. These properties make such instruments attractive for microsatellites. We have previously shown that microbolometer arrays have sufficient sensitivities for a variety of infrared hyperspectral applications (Lucey et. al., 2004; Lucey et. al., 2008; Crites et. al., 2012; Gabrieli et. al., 2016, Honniball et. al., 2017). Instruments including the Thermal InfraRed Compact Imaging Spectrometer (TIRCIS) (Crites, et al., 2015), the Thermal Hyperspectral Imager (THI) (Gabrieli et. al., 2016), and the Miniaturized Infrared Detector of Atmospheric Species (MIDAS) (Honniball et. al., 2017) use imaging interferometers (e.g. Fabry-

Perot or Sagnac interferometer, respectively) coupled with microbolometers to attain hyperspectral images in the Long-Wave InfraRed (LWIR) from 7-14 μm and Mid-Wave InfraRed (MWIR) from 3-5 μm. TIRCIS, THI, and MIDAS are used for a variety of applications from atmospheric gas detection to lava flow irradiance measurements.

Commercial microbolometers are designed for high contrast broadband imaging, not for spectroscopy. The requirements for HSI are not the same as for thermal imaging. For thermal imaging the detailed spectral response of a detector is not of high importance, and there is even some desire to be less responsive at some wavelengths to avoid atmospheric issues. However, for spectroscopy and therefore HSI, the spectral response of a detector is important and should be spectrally flat. Knowledge of a detector's spectral response is important to match the detector to spectral applications. Spectral response is a measure of how well a detector responds to light with wavelength. It depends on a number of factors such as the detector coating and spectral transmission of the optics. To support our spectral applications, we embarked on a campaign to characterize the spectral response of four commercially available uncooled microbolometers and one cooled photon detector. A list of the detectors and their specifications can be found in Table 1. Three of the microbolometers (FLIR Photon, FLIR Tau, Sofradir Pico) are sensitive to the LWIR while one is sensitive to both MWIR and LWIR (INO). The cooled photon detector (IRCamera) is sensitive to the MWIR. We also measured the noise equivalent differential temperature (NEdT) of the detectors with a 147nm narrow band filter at 10.8 μm for the Photon, Tau, Sofradir, and INO microbolometers and at 3.8 μm for the IRCamera and INO detectors in order to quantify their relative sensitivities. The narrow band NEdT of the INO microbolometer was measured at two wavelengths due to its response in both the MWIR and LWIR.

Table 1: List of detectors measured and their specifications used in this campaign. The narrow band NEdT is also reported.

Camera	**Wavelength Region**	**Detector technology**	**Pixel count**	**Pixel size**	**NB NEdT (mK)**	**NB NEdT temperature**	**Frame rate**
FLIR Photon	7-14 μm	VOx	324x256	38 μm	36 @ 10.8 μm	90°C	30 Hz
FLIR Tau	7-14 μm	VOx	640x512	17 μm	99 @ 10.8 μm	90°C	60 Hz
Sofradir Pico	7-14 μm	a-Si	640x480	17 μm	77 @ 10.8 μm	90°C	60 Hz
INO MircoXcam	3-14 μm	VOx	384x288	35 μm	19 @ 10.8 μm 38 @ 3.81 μm	90°C 60°C	50 Hz
IRCamera 803	3 – 5.2 μm	InSb	320x240	30 μm	64 @ 3.81 μm	60°C	30 Hz *itime=1ms

*The IRCamera photon detector measurements were obtained with no thermal background suppression filter, the integrations were limited by that background.

METHODOLOGY

Radiance Source Calibration

Characterizing the spectral response of the microbolometers and photon detector required a calibrated, narrow band source of irradiance. This was accomplished by using a monochromator illuminated by a blackbody source with known temperature calibrated with a broadband infrared detector with flat spectral response. To provide sufficient flux through the very narrow band, the blackbody was operated at 700°C. To calibrate the narrow band irradiance output by the monochromator we used a radiometry system with a pyroelectric detector with a known flat spectral response. The signal from the blackbody was modulated with a chopper wheel and measured with a lock-in amplifier to reduce noise. This system can be seen in Figure 1 and 2. Because of the wavelength ranges of the detectors used in this campaign, it was required that the output of the monochromator be calibrated from 2 to 14 μm. The monochromator allows only a single wavelength of irradiance through a narrow slit which was set to a width of 600 μm giving the monochromator resolutions of 32 nm from 2 to 5μm, 64 nm from 4 to 9 μm, and 96 nm from 7 to 14 μm depending on the grating used. The output wavelength was adjusted by tilting the diffraction grating in the monochromator with a manual crank. Diffraction gratings are only efficient over about a factor of two in wavelength, so three gratings were selected. In order to calibrate the monochromator from 2 to 14 μm a series of gratings and order separating filters were used for specified wavelength ranges as listed in Table 2. Since the monochromator uses diffraction gratings that diffracted several wavelengths at the same angle, order separating filters were necessary to block second order irradiance from being measured by the detectors which would have caused an erroneous increase in the signal measured. Commercial parts used for spectral response characterization can be found in Table 3.

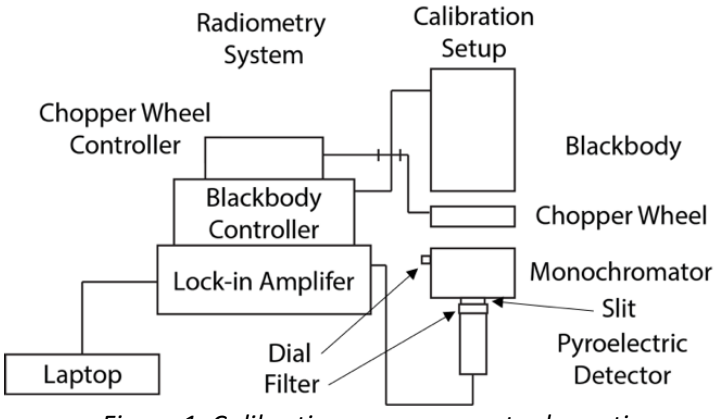

Figure 1: Calibration measurement schematic.

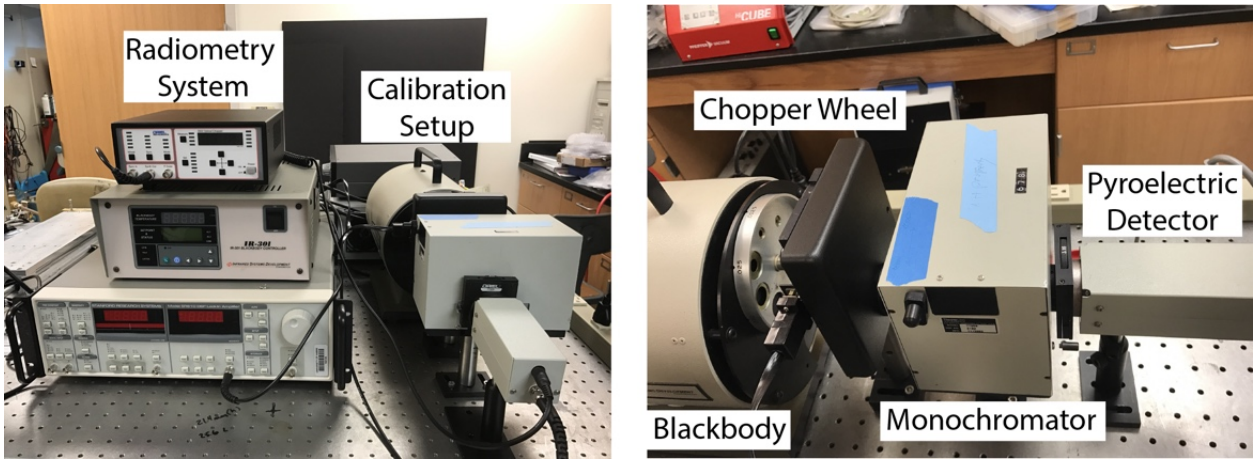

Figure 2: Laboratory calibration setup. Radiometry system looking through the monochromator to the hot blackbody.

Table 2: List of grating and order separating filters used for each wavelength range

Wavelength Region	**Grating part number**	**Blaze**	**Line density**	**Order separating filter**	**Resolution**	**Detector**
2 -5 µm	Oriel 77301	3.5 µm	150 (l/mm)	>2.4 µm	32 nm	IRCamera, INO
4 – 9 µm	Oriel 77302	7 µm	75 (l/mm)	>4.5 µm	64 nm	IRCamera, INO
7 – 14 µm	Oriel 77303	12 µm	50 (l/mm)	>7.3 µm	96 nm	INO, Photon, Tau, Sofradir

Table 3: List of commercial parts used for characterizing spectral response.

Spectral response use	**Commercial part**	**Part number**
Irradiance source	Infrared Systems NIST traceable high temperature blackbody	IR-564
Narrow band source	Oriel Monochromator	77250-FH
Calibration instrument	Newport Lock-in amplifier radiometric system with a pyroelectric detector	LIDA-SRS-KIT-120V DET-L-PYK5-R-P

For each camera, we measured its response to the radiant output of the monochromator/blackbody system, and normalized this measurement to the response of the spectrally flat pyroelectric detector to the output of the monochromator at the same wavelength. The radiance output by the monochromator (R_{mono}) is a function of the radiance output by the blackbody (L_{BB}), transmission through the monochromator (τ_{mono}), transmission through the atmosphere (τ_{atm}), and the spectrally flat gain of the pyroelectric (G_{pyro}) as represented by Equation 1.

$$Eq.1 \quad R_{mono}\left(\frac{V}{W}\right) = L_{BB} * \tau_{mono} * \tau_{atm} * G_{pyro}\left(\frac{V}{W}\right)$$

Physically, the radiance output by the monochromator was measured as the difference between the monochromator with its slit open and slit closed, blocking the radiance from the blackbody. This procedure was used for both the calibration of the monochromator and the spectral response measurements of the detectors. Shown in Figure 3 is an image representation using an imaging interferometer of this slit open minus slit closed process.

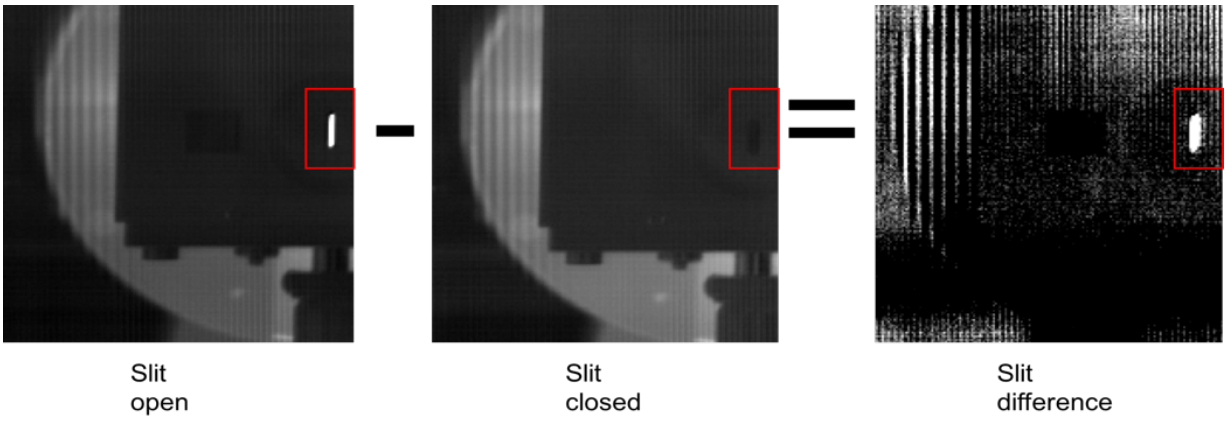

Figure 3: The red box indicates the monochromator slit. The left is the slit open, center is closed, and the right is the difference between the slit opened and closed.

Monochromator Calibration Curve

The output of the monochromator can be seen in Figure 4a-e as measured by pyroelectric detector. Because the pyroelectric detector has a flat response, the shape of the curves is due to the shape of the blackbody illuminator (peaking at 3 μm) and the spectral efficiency of the monochromator. The MWIR and LWIR calibration curves can be seen in Figures 4a and 4b,

respectively, while the full 2 to 14 μm curve is given in 4c. The curve in 4a was used to calibrate the IRCamera, 4b was used for the Photon, Tau, and Sofradir microbolometers, and 4c was used for the INO microbolometer. In order to make the full 2 to 14 μm curve we pieced together measurements using different grating and order separating filter combinations as listed in Table 2. Figures 4c and 4d indicate where the change in grating and filter occurred and 4c shows the overlap of each wavelength range. The transition points were selected based on its effect on the INO microbolometer data and which transitions had the least change in radiance.

In both the MWIR calibration curve and the full calibration curve there is a prominent absorption feature at roughly 4.2 μm due to atmospheric CO_2. There is also a slight indication of water absorption at 3 μm and a strong water feature at 6 μm which can both be seen in Figure 4e. The 3 μm feature is weak because the output of the monochromator is decreasing in radiance output. To verify these absorption features we ran an atmospheric transmission model (MODTRAN) using a path length of 500 mm (the path length between the blackbody and detectors), standard tropical atmospheric conditions, and a CO_2 concentration of 1200 ppmv (consistent with indoor CO_2 concentrations) as seen in 4f. The blue bands in 4e and 4f represent water absorption and the purple bands, also seen in 4a, represent CO_2. From this analysis we conclude that the narrow spectral features in the calibration curve are due to atmospheric gases.

Detector Spectral Response

Spectral response of the microbolometers and photon detectors is found by measuring each detector's response to the narrow band irradiance from the monochromator expressed in Equation 2. The raw response of the cameras is the same as for the pyroelectric detector.

$$Eq.2 \quad R_{detector} = L_{BB} * \tau_{mono} * \tau_{atm} * G_{detector} \left(\frac{DN}{W}\right)$$

The calibrated spectral response measured by the detectors is a function of the monochromator output and must be divided by the calibration curves discussed in the previous section. This ratio, shown in Equation 3, removes the transmission of the monochromator, the spectral variation of the blackbody, and to a large degree the absorption due to the atmosphere, leaving us with the gain measured by the detector divided by the gain measured by the pyroelectric detector.

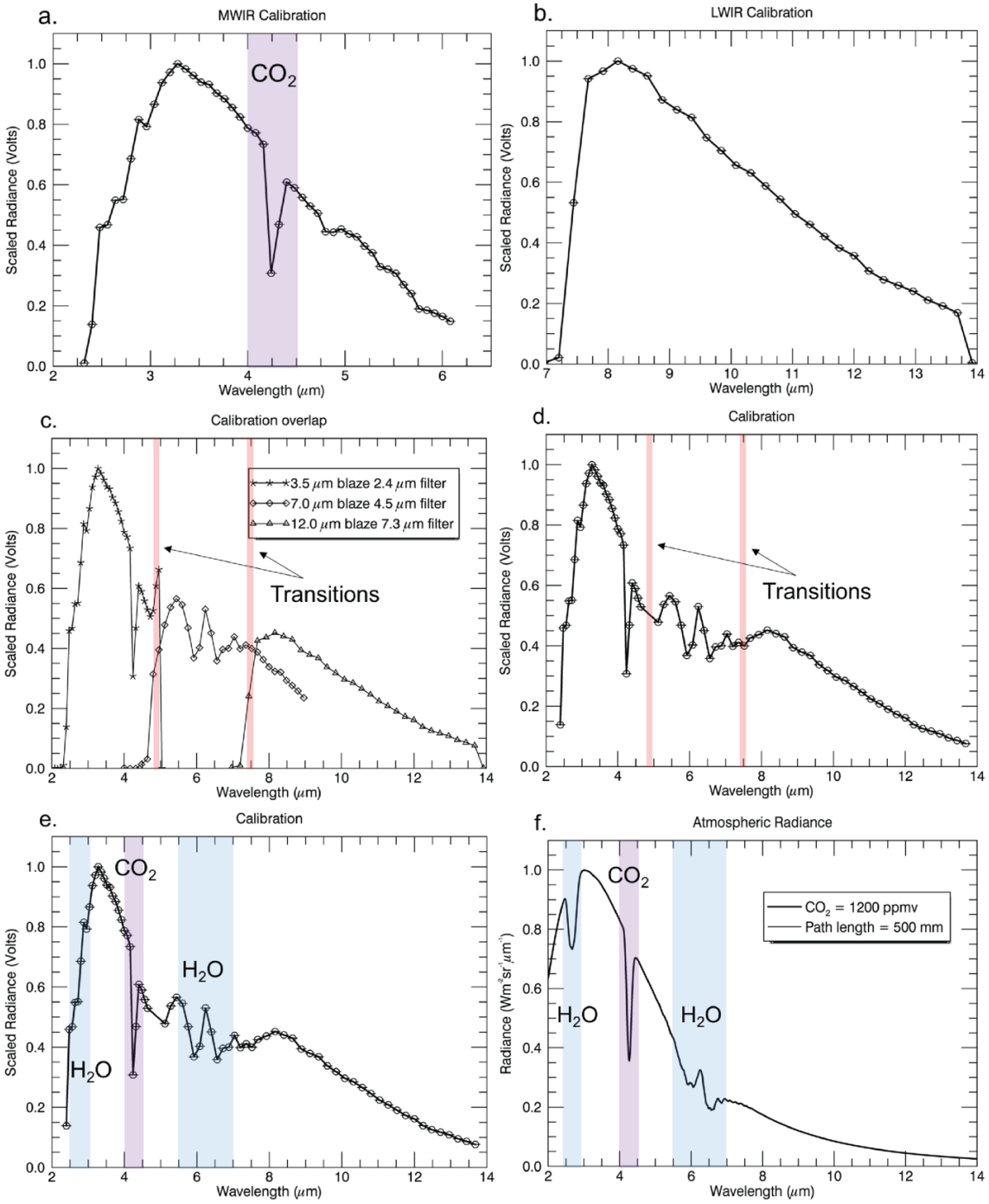

Figure 4: MWIR and LWIR calibration curves of the monochromator (a & b respectively). The MWIR curve has a prominent CO_2 absorption feature at 4.2 μm and a shallow water absorption at 3 μm. c & d) Full calibration curve of the monochromator from 2 to 14 μm. This curve is made up of three separate curves pieced together. The transition from one curve to the next is highlighted by the red bar. In this curve you can see the CO_2 absorption feature as well as water absorption at 3 and 6 μm. C shows the overlap of the three curves. e & f) show the effects of atmospheric absorptions on the calibration curve in e. f was produced from MODTRAN using a path length of 500 mm, standard tropical atmospheric conditions and a CO_2 concentration of 1200 ppmv.

$$Eq: 3 \quad SR_{detector}\left(\frac{DN}{V}\right) = \frac{R_{detector}}{R_{mono}} = \frac{G_{detector}\left(\frac{DN}{W}\right)}{G_{pyro}\left(\frac{V}{W}\right)}$$

Measurement of the camera detector's response to the monochromator is acquired in the same fashion as the calibration data: by imaging the slit open and closed and taking the difference of the two to find the total radiance measured by the detector at a certain wavelength. Figure 5a shows a schematic of the spectral response experiment while 5b shows the actual set up using the INO microbolometer, monochromator, and blackbody. The path length between the detector and the blackbody must be the same as it was for the calibration tests to accurately compensate for atmospheric absorption in the detector data. Due to this constraint, we set the pyroelectric detector in front of the monochromator at a position that was easily repeatable with the cameras. For the detector spectral response tests the chopper wheel was not needed so it was removed but the blackbody and monochromator were left in the same position to preserve the path length. The grating and order separating filters were selected based on the wavelength range of the detector and show in Table 2.

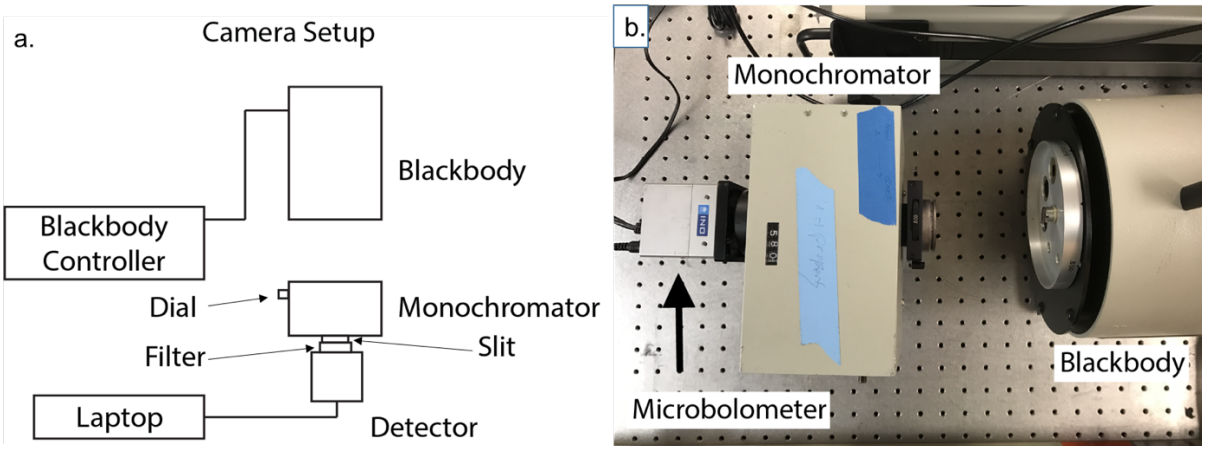

Figure 5: On the left is a schematic of the detector spectral response experiment setup. On the right is an image of the INO microbolometer, monochromator and blackbody setup for measurements.

SPECTRAL RESPONSE RESULTS

The normalized spectral response curves for the four microbolometers and the photon detector can be seen below in Figure 6, 7 and 8. All the spectral response plots show the calibrated response as the solid line with circles indicating the sampling while the raw response of the camera to the

monochromator is a dashed line. The calibrated curve was calculated by taking the raw response of the detectors and dividing by the appropriate calibration curve measured by the pyroelectric detector. Figures 6a show the spectral response of the IRCamera photon detector in the MWIR. The calibrated curve of the detector is expected from an Indium Antimonide (InSb) photon detector, Figure 6b shows a textbook example (Hudson, 1969). The rising slope of the InSb curve is due to the increasing number of photons per watt with increasing wavelength, and the sudden drop is where the energy of the infrared photons drop below the band gap of indium antimonide. For the complete curve for the IRCamera we pieced together two of the calibration curves and the transition is indicated by the red bar.

The raw response of the IRCamera photon detector shows the CO_2 feature mentioned earlier in the discussion of the calibration curve. In the calibrated curve the CO_2 feature location has a residual anomaly in the spectral response. This artifact is caused by; 1) the IRCamera being at a slightly different path length from the blackbody than the pyroelectric detector used for calibrations. This can cause the strength of the CO_2 feature to vary. 2) The manual dial position on the monochromator is not perfectly reproducible between the calibration data and the detector data, causing the CO_2 feature to shift apparent wavelengths. 3) The CO_2 concentration is the room could have changed between the day the calibration data was taken and the day the IRCamera data was taken, causing the strength of the CO_2 feature to vary. Due to these three effects the CO_2 feature does not calibrate out perfectly and causes an anomaly at 4.2 μm.

The response of the three LWIR microbolometers, Photon, Tau, and Sofradir, are shown in Figure 7a-c, respectively. Both the Photon and the Tau use VOx technology while the Sofradir uses a-Si. The Photon microbolometer shows a smooth spectral response curve that increases from 8 μm to ~9.5 μm then flattens out from 9.5 to 12.5 μm where it starts to slightly decrease in spectral response. The long wavelength decrease is typical for a germanium window the Photon camera uses. The Tau microbolometer shows spectral response that is highly variable across the whole 7 to 14 μm range. The Sofradir microbolometer's spectral response drops sharply below 8 μm, due to a filtering window included with the detector to allow for sharper thermal imaging. The Sofradir camera shows a flat spectral response from 8 to ~12 μm; past 12 μm the spectral response shows high but variable response.

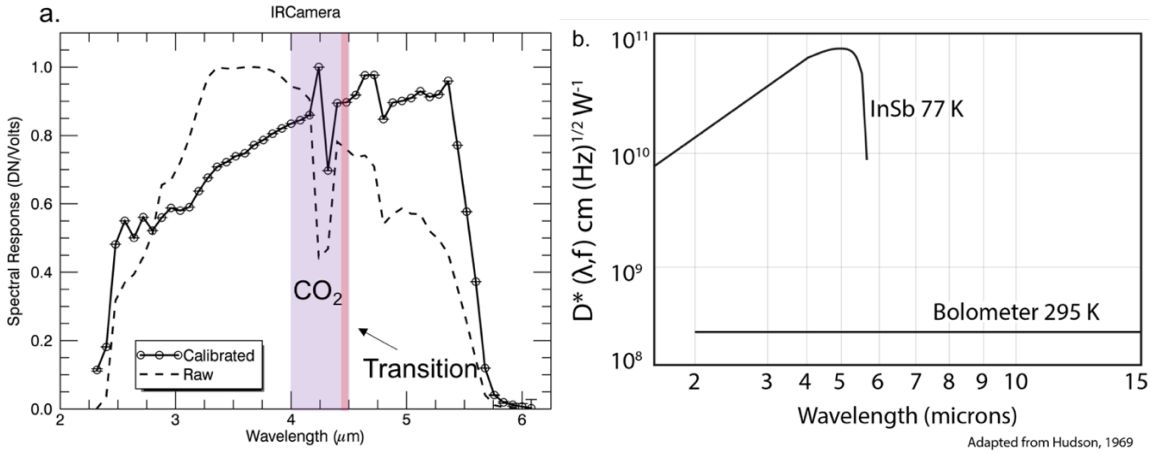

Figure 6: On the left is the spectral response of the MWIR IRCamera InSb photon detector. The dashed line is the raw response of the camera to the output by the monochromator. The solid line is the raw response divided by the MWIR calibration curve using the spectrally flat pyroelectric detector. The anomaly at 4.2 μm in the calibrated spectral response curve is due to varying path length, varying CO_2 concentration in the room, and dial position on the monochromator. The spectral response curve was pieced together from two grating and filter settings (3.5 μm grating with 2.4 μm order separating filter and the 7 μm grating with the 4.5 μm order separating filter). The transition from one curve to the next is shown by the red bar. On the right is the relative spectral response of InSb photon detectors and a bolometer adapted from Hudson, 1969.

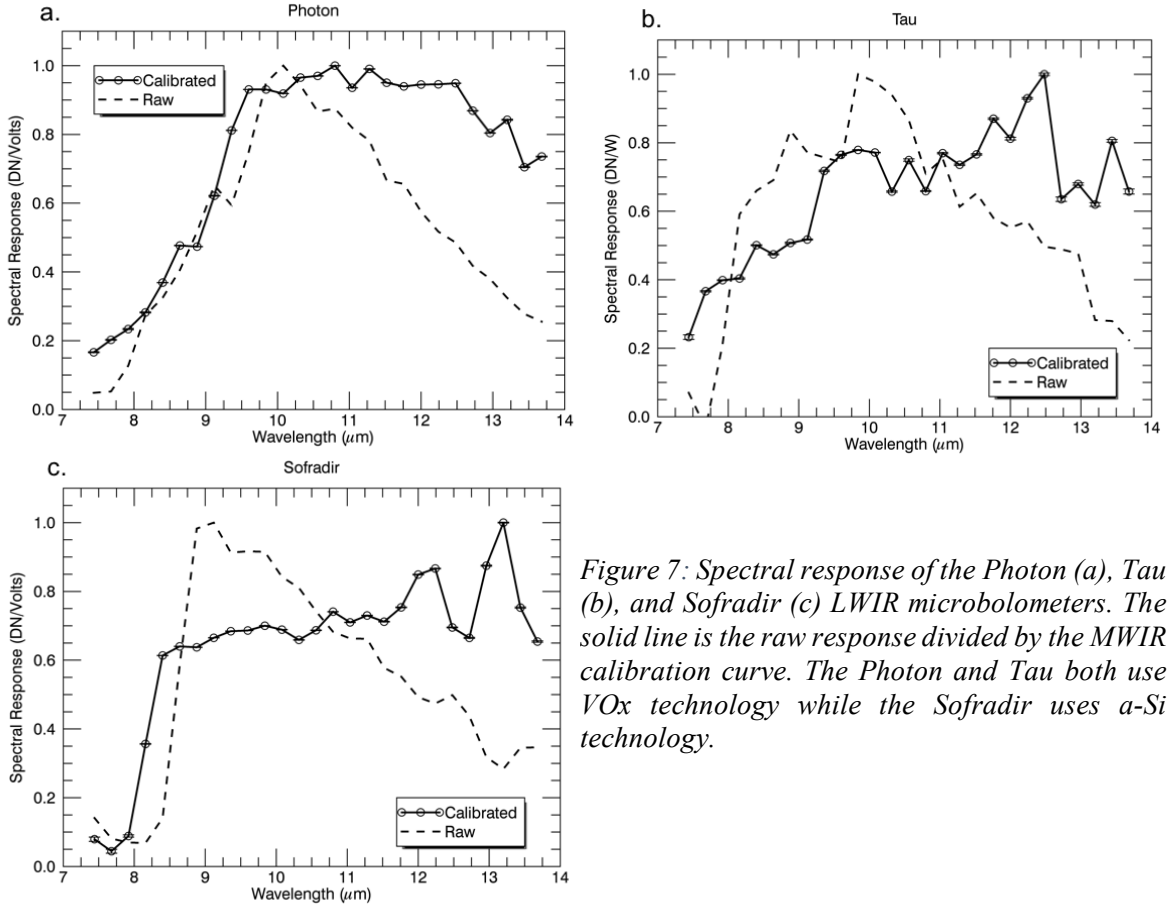

Figure 7: Spectral response of the Photon (a), Tau (b), and Sofradir (c) LWIR microbolometers. The solid line is the raw response divided by the MWIR calibration curve. The Photon and Tau both use VOx technology while the Sofradir uses a-Si technology.

Lastly, the INO microbolometer spectral response is shown in Figure 8. Since the INO camera is designed to be sensitive to both the MWIR and LWIR, the spectral response data was taken in three grating and filter combinations as was done for the full range calibration curve. The grating and filter combinations can be found in Table 2. The spectral response curve for the INO camera was pieced together in the same manner as the calibration curve. The transitions are shown by the red bars in Figure 8. Again, the raw response output by the monochromator and measured by the INO microbolometer is seen as a dashed line while the calibrated spectral response is the solid line. Our results show that the INO microbolometer has a flat spectral response from 3 to 14 μm with a decrease near 13 μm due to a germanium window. New technology developed by INO using a thin but extremely absorptive coating of gold black film has been introduced by Fisette et. al., 2017. The gold black coating enables a highly sensitive imaging detector with nearly flat spectral response (Fisette et. al., 2017). Because the INO is sensitive to the MWIR we see the CO_2 feature at 4.2 μm in the raw data and the anomaly caused by differences in path length, dial position, or varying CO_2 concentrations. There is another anomaly around 4.8 μm which corresponds to a transition from one curve to another. This anomaly is due to the calibration curve and the INO raw spectral response transitions having discrepancies between the curves. Overall the INO microbolometer shows a wider and flatter spectral response for both the MWIR and LWIR compared to the other microbolometers as well as the photon detector.

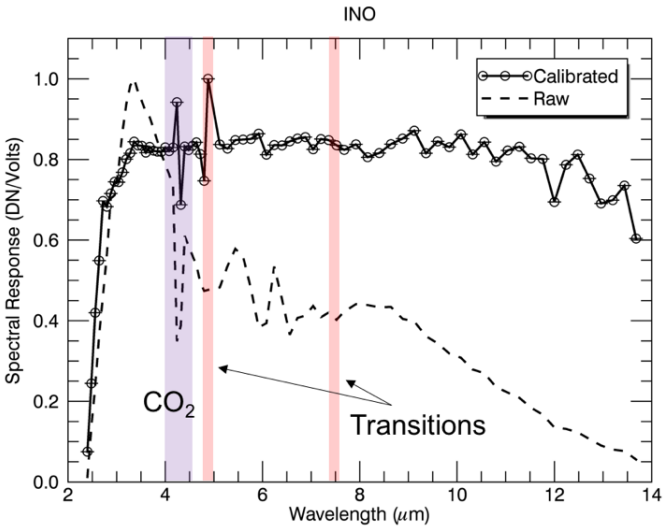

Figure 8: Spectral response of the INO microbolometer over the MWIR and LWIR. The solid line is the raw response divided by the MWIR calibration curve. The INO uses gold black technology to achieve a flat spectral response. The anomaly at 4.2 μm in the calibrated spectral response curve is due to varying path length, varying CO_2 concentration in the room, and dial position on the monochromator. The spectral response curve was pieced together from the three grating and filter settings listed in Table 2. The transition from one curve to the next is shown by the red bar.

The spectral response curves are normalized and do not say anything about how the cameras compare with each other in terms of sensitivity. While the spectral response is of high interest, especially for HSI, the sensitivity of each camera is crucial.

The typical sensitivity metric for thermal cameras is NEdT, usually measured over the full atmospheric window. However, we have shown strong variations in spectral response that would bias understanding of the intrinsic sensitivity of each camera. For this reason, we measured the NEdT over a very narrow band. We can then compare the spectral sensitivities of the cameras by scaling each camera to its narrow band NEDT at the measured wavelength. Each detector's spectral response was then scaled by the ratio:

$$\frac{INO\ narrow\ band\ NEdT}{Detector\ narrow\ band\ NEdT}$$

This provided the relative spectral response of each detector and can be seen in Figure 9. These plots show that the INO microbolometer performs two times better than the IRCamera photon detector and the FLIR Photon microbolometer and four times better than the Tau and Sofradir microbolometers. The IRCamera was set to an integration time of 1 ms in order to avoid saturation and could be the cause of the lower sensitivity.

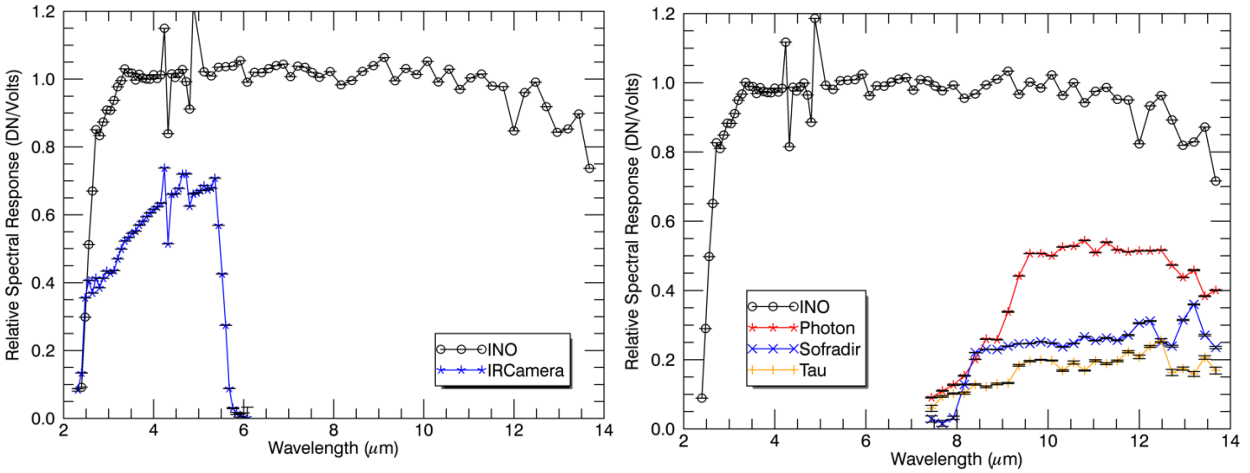

Figure 9: Relative spectral response of the five cameras measured. The left shows the relative response of the INO microbolometer and the IRCamera photon detector normalized to 3.8 μm and scaled to narrow band NEdT measurements at 3.8 μm with a blackbody temperature of 60°C. The right shows the relative spectral response of the four microbolometers normalized to 10.5 μm and scaled to narrow band NEdT measurements at 10.8 μm with a blackbody temperature of 90°C.

CONCLUSION

The spectral response and sensitivity of cameras is clearly critically important for determining their use for spectral applications. We have measured the spectral response for several microbolometer cameras and a photon detector. Of the cameras tested, we find that the INO microbolometer with a thin gold black film has the highest sensitivity, largely due to its large pixel size, and features a flat spectral response in both the MWIR and LWIR. All other cameras, including the IRCamera photon detector, are two to four times less sensitive than the INO microbolometer. For HSI the high sensitivity and flat spectral response over the wide wavelength range of the INO microbolometer makes it ideal for many spectroscopic applications. It also has the advantage of being uncooled with a small footprint making it ideal for microsatellites.

REFERENCES

[1] Fisette, B., Tremblay, M., Oulachgar, H., Généreux, F., Béland, D., Beaupré, P., Julien, C.,Gay, D., Deshaies, S., Terroux, M., Tremblay, B., Dufour, D., Alain, C., "Novel vacuum packaged 384×288 broadband bolometer FPA with enhanced absorption in 3-14μm wavelength range," Proc. SPIE 10177, Infrared Technology and Applications XLIII, 101771R (2017).

[2] Crites, S.T., Wright, R., Lucey, P.G., Chan, J., Gabrieli, A., Garbeil, H., Horton, K.A., Imai-Hong, A.K.R., Pilger, E.J., Wood, M., and Yoneshige, L., "The Thermal Infrared Compact Imaging Spectrometer (TIRCIS): a follow-on to the Space Ultra Compact Hyperspectral Imager (SUCHI)." Proc. SPIE 9469, Sensors and Systems for Space Applications VIII, 94690R (2015).

[3] Einstein, A. "Concerning an Heuristic Point of View Toward the Emission and Transformation of Light." *Annalen der Physik* 17 (1905): 132-148.

[4] Gabrieli, A., Wright, R., "Characterization and initial field test of an 8–14 μm thermal infrared hyperspectral imager for measuring SO2 in volcanic plumes." Bulletin of Volcanology, 78(73), 1-13 (2016).

[5] Honniball, C.I., Wright, R., Lucey, P.G., "MWIR hyperspectral imaging with the MIDAS instrument." Proc. SPIE 9819, Infrared Technology and Applications XLII. in prep., 10177-17 (2017).

[6] Hudson, "Infrared system engineering" (1969)

[7] Lucey, P.G., Horton, K.A., Williams, T., "Performance of a long-wave infrared hyperspectral imager using a Sagnac interferometer and an uncooled microbolometer array." Applied optics, 47(28), 107-13 (2008).

[8] Lucey, P.G., Wilcox, B.B., "Mini-SMIFTS: an uncooled LWIR hyperspectral sensor." Optical Science and Technology. SPIE's 48th Annual Meeting. International Society for Optics and Photonics, 275-282 (2004).

[9] Petitweg, C. (2008). Applications of Thermal Imaging Cameras. FLIR Media.